

Persistence of antiferromagnetic order upon La substitution in the $4d^4$ Mott insulator Ca_2RuO_4 D. Pincini,^{1,2,*} S. Boseggia,¹ R. Perry,¹ M. J. Gutmann,³ S. Riccò,⁴ L. S. I. Veiga,¹ C. D. Dashwood,¹ S. P. Collins,² G. Nisbet,² A. Bombardi,^{2,5} D. G. Porter,² F. Baumberger,^{4,6} A. T. Boothroyd,⁵ and D. F. McMorrow¹¹*London Centre for Nanotechnology and Department of Physics and Astronomy, University College London, Gower Street, London WC1E6BT, United Kingdom*²*Diamond Light Source Ltd., Diamond House, Harwell Science & Innovation Campus, Didcot, Oxfordshire OX11 0DE, United Kingdom*³*ISIS Neutron and Muon Source, Science and Technology Facilities Council, Rutherford Appleton Laboratory, Didcot OX11 0QX, United Kingdom*⁴*Department of Quantum Matter Physics, University of Geneva, 24 Quai Ernest-Ansermet, 1211 Geneva 4, Switzerland*⁵*Department of Physics, University of Oxford, Clarendon Laboratory, Oxford OX1 3PU, United Kingdom*⁶*Swiss Light Source, Paul Scherrer Institut, CH-5232 Villigen PSI, Switzerland*

(Received 15 May 2018; revised manuscript received 28 June 2018; published 26 July 2018)

The chemical and magnetic structures of the series of compounds $\text{Ca}_{2-x}\text{La}_x\text{RuO}_4$ [$x = 0, 0.05(1), 0.07(1), 0.12(1)$] have been investigated using neutron diffraction and resonant elastic x-ray scattering. Upon La doping, the low-temperature *S-Pbca* space group of the parent compound is retained in all insulating samples [$x \leq 0.07(1)$], but with significant changes to the atomic positions within the unit cell. These changes can be characterized in terms of the local RuO_6 octahedral coordination: with increasing doping, the structure, crudely speaking, evolves from an orthorhombic unit cell with compressed octahedra to a quasitetragonal unit cell with elongated ones. The magnetic structure on the other hand, is found to be robust, with the basic $\mathbf{k} = (0, 0, 0)$, \mathbf{b} -axis antiferromagnetic order of the parent compound preserved below the critical La doping concentration of $x \approx 0.11$. The only effects of La doping on the magnetic structure are to suppress the A-centred mode, favoring the B mode instead, and to reduce the Néel temperature somewhat. Our results are discussed with reference to previous experimental reports on the effects of cation substitution on the d^4 Mott insulator Ca_2RuO_4 , as well as with regard to theoretical studies on the evolution of its electronic and magnetic structure. In particular, our results rule out the presence of a proposed ferromagnetic phase, and suggest that the structural effects associated with La substitution play an important role in the physics of the system.

DOI: [10.1103/PhysRevB.98.014429](https://doi.org/10.1103/PhysRevB.98.014429)**I. INTRODUCTION**

Doped Mott insulators host a plethora of novel electronic phases including unconventional superconductivity, pseudo-gap states, charge density wave order, etc. [1]. Elemental substitution offers the unique possibility to tune two of the fundamental parameters of a strongly correlated electron system, i.e., the one-electron bandwidth (*bandwidth control*) and the band filling (*filling control*), and thus allows a rich phase diagram of electronic and magnetic states to be accessed [2]. The doping evolution of the magnetic ground state of the parent compound, which is usually dictated by oxygen-mediated superexchange interactions, varies between different systems. In perovskite manganites, the parent antiferromagnetic (AFM) order develops into a ferromagnetic (FM) phase hosting giant magnetoresistance [2]. On the other hand, in both $S = 1/2$ cuprates [1] and $J_{\text{eff}} = 1/2$ iridates [3–6], doping suppresses long-range AFM order leading to the formation of incommensurate spin-density wave order [7–10] with a conventional paramagnetic (PM) metal eventually emerging.

Particularly interesting is the case of Mott insulators containing d^4 transition metal ions (such as Ru^{4+} , Os^{4+} , and Ir^{5+}), where moderate spin-orbit coupling (SOC) $\lambda(\mathbf{S} \cdot \mathbf{L})$ is expected

to stabilize a nonmagnetic $J_{\text{eff}} = 0$ singlet [11]. In this case, magnetic order can result from the condensation of magnetic excited states driven by intersite interactions [12, 13], provided that the exchange coupling is strong enough to overcome the energy of promotion of the ion to the excited state (separated from the ground state by λ). This unusual singlet magnetism has been recently predicted to give rise to a rich phase diagram as a function of electron doping [14]: here, the magnetic ground state was found to strongly depend on the relative strength of the hopping integral t_0 , the SOC constant λ , and the correlation energy U . In particular, through electron doping of the parent AFM phase, the system is expected to evolve towards either a FM or a PM phase depending on the size of λ , with possibility of triplet superconductivity in the former case.

Ca_2RuO_4 is a prominent candidate for the realization of $J_{\text{eff}} = 0$ ($L_{\text{eff}} = 1$, $S = 1$) singlet magnetism [13–15]. However, there is still controversy as to the precise role played by SOC in the exchange between Ru^{4+} ($4d^4$) magnetic moments. Evidence supporting the proximity of Ca_2RuO_4 to a $J_{\text{eff}} = 0$ ground state was provided by a recent inelastic neutron investigation [15], which reported the existence of the amplitude (Higgs) mode in the magnetic excitations spectrum expected to arise from the condensation of the excited $J_{\text{eff}} = 1$ triplet. Other studies accounted for the spin-wave spectrum by a more conventional $S = 1$ Heisenberg-like magnetic-exchange model, where a finite spin-wave gap is opened by the SOC-induced

*davide.pincini.14@ucl.ac.uk

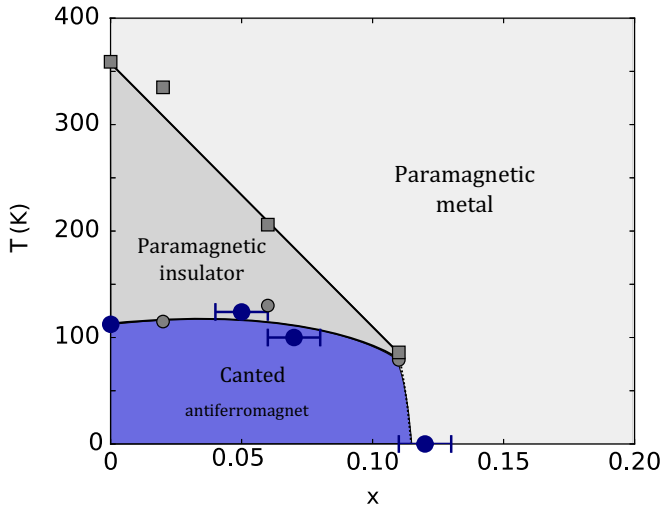


FIG. 2. $\text{Ca}_{2-x}\text{La}_x\text{RuO}_4$ temperature-doping phase diagram. The filled squares represent the temperatures (from Ref. [27]) at which the transition between the high-temperature quasitetragonal metallic phase (*L-Pbca*) and the low-temperature orthorhombic one (*S-Pbca*) occurs. The small and large filled circles are the Néel temperatures taken from Ref. [27] and derived from our bulk magnetization measurements [30], respectively. The error bars reflect the uncertainty in the doping level measured by means of EDX.

a pyrolytic graphite (002) crystal in 90° -scattering geometry placed upstream with respect to an APD detector. This provided a scattering angle of $\theta = 40.66^\circ$ and $\theta = 38.51^\circ$ at the L_3 and L_2 edges, respectively. The total scattered intensity was measured using a Pilatus 100K area detector in ultrahigh gain mode. The samples were cooled down below the Néel transition temperature by means of a closed-cycle cryostat.

The crystal structure characterization was carried out by means of the Laue single-crystal diffractometer at the SXD instrument of the ISIS Neutron and Muon Source (Didcot, UK) [33] while XANES spectra at the Ru L edges were measured at the ID12 beamline of the European Synchrotron Radiation Facility (Grenoble, France) in total-electron yield detection mode and used to correct the REXS data for self-absorption.

III. SAMPLE GROWTH AND CHARACTERIZATION

Single crystals of $\text{Ca}_{2-x}\text{La}_x\text{RuO}_4$, with $x = 0, 0.05(1), 0.07(1),$ and $0.12(1)$ [corresponding to the nominal dopings $x = 0, 0.05, 0.10,$ and $0.15,$ respectively], were grown through the floating zone technique using a Crystal System Corporation FZ-T10000-H-VI-VPO-IHR-PC four-mirror optical furnace. Samples were prepared in 90% oxygen pressure, and the initial Ru concentration in the polycrystalline rods was about 20% higher than the nominal value to compensate for evaporation during the growth. The doping level was determined by means of energy-dispersive x-ray (EDX) spectroscopy, while the bulk magnetic properties were characterized through magnetization measurements performed using a Quantum Design MPMS 3 setup [30]. The crystals used for the REXS measurements were approximately $1 \times 1 \text{ mm}^2$ in size, with a crystal mosaic of about 0.05° as extracted from the FWHM of the Bragg peak rocking curve. Powder samples of the same compounds were

also synthesised between 1400°C and 1500°C (the temperature was increased with the La content) and 1% O_2 atmosphere. The conditions were adapted from Ref. [34]. The parent compound ($x = 0$) displays a well-documented metal to insulator transition (MIT) at $T_{\text{MIT}} = 357 \text{ K}$ concomitant to a first-order structural transition from a high-temperature quasitetragonal phase with a long c axis (*L-Pbca*) to a low-temperature orthorhombic one with a short c axis (*S-Pbca*) [27,34–36]. Below $T_N \approx 110 \text{ K}$, a phase transition to the basal plane C-AFM state also occurs [19,27–29,34,35,37]. La substitution causes the MIT and Néel temperature to decrease and be ultimately completely suppressed at a doping concentration slightly higher than $x = 0.11(2)$ [27]. The corresponding temperature-doping phase diagram is shown in Fig. 2. Here, we report the Néel temperature derived from our bulk magnetization measurements (large filled circles with errorbars) [30] along with the results of the magnetization (small filled circles) and resistivity (filled squares) data collected by Fukazawa *et al.* [27].

IV. RESULTS

A. Structural characterization

The structural properties of $\text{Ca}_{2-x}\text{La}_x\text{RuO}_4$ as a function of the doping level were investigated by means of single crystal neutron diffraction at $T = 10 \text{ K}$. The doped samples retain the same space group (*Pbca*, No.61) of the parent compound. However, the different Shannon radii of the La^{3+} ($r = 1.22 \text{ \AA}$) and Ca^{2+} ($r = 1.18 \text{ \AA}$) ions [27,38] result in significant structural changes. The unit cell of Ca_2RuO_4 is shown in Fig. 1(a) along with the definition of relevant structural parameters, while the main results of the neutron data refinement are summarized in Fig. 3. The structural changes can be described in terms of the following four parameters: (i) unit cell distortion $1 - \frac{a}{b}$, where a and b are the in-plane lattice constants of the *Pbca* unit cell; (ii) octahedral distortion $1 - \frac{r_x+r_y}{2r_z}$, where $r_{x,y}$ and r_z are the in-plane and apical Ru-O bond lengths of the RuO_6 octahedra, respectively; (iii) Ru-O-Ru bond angle; (iv) octahedral tilt angle away from the crystallographic c axis. The unit cell of the parent compound at low temperature is orthorhombic, with a b lattice parameter elongated by 4.4% with respect to a . Large distortions away from the perfect perovskite structure ($1 - \frac{r_x+r_y}{2r_z} = 0$, Ru-O-Ru angle = 180° and tilt angle = 0°) are also present: the RuO_6 octahedra are significantly compressed along the local z axis ($1 - \frac{r_x+r_y}{2r_z} < 0$) and display both a sizable rotation around the apical Ru-O bond direction and tilt away from the c axis [Fig. 1(a)]. La substitution is found to cause a reduction of the orthorhombicity of the unit cell ($1 - \frac{a}{b} \rightarrow 0$), in agreement with a previous study [27], and an elongation of the octahedral cage ($1 - \frac{r_x+r_y}{2r_z} > 0$): this results in the phase diagram of Fig. 3(a), where for increasing doping levels, the system evolves from an orthorhombic cell with compressed octahedra ($x = 0, 0.05$) to a quasitetragonal cell with elongated ones ($x = 0.07, 0.12$). The rotations of the octahedral cage are also reduced [Fig. 3(b)] and the structure tends to relax towards the undistorted perovskite lattice. Further details on the structural refinement and additional room temperature results are reported in Refs. [30,39], which the reader is referred to for the corresponding CIF files.

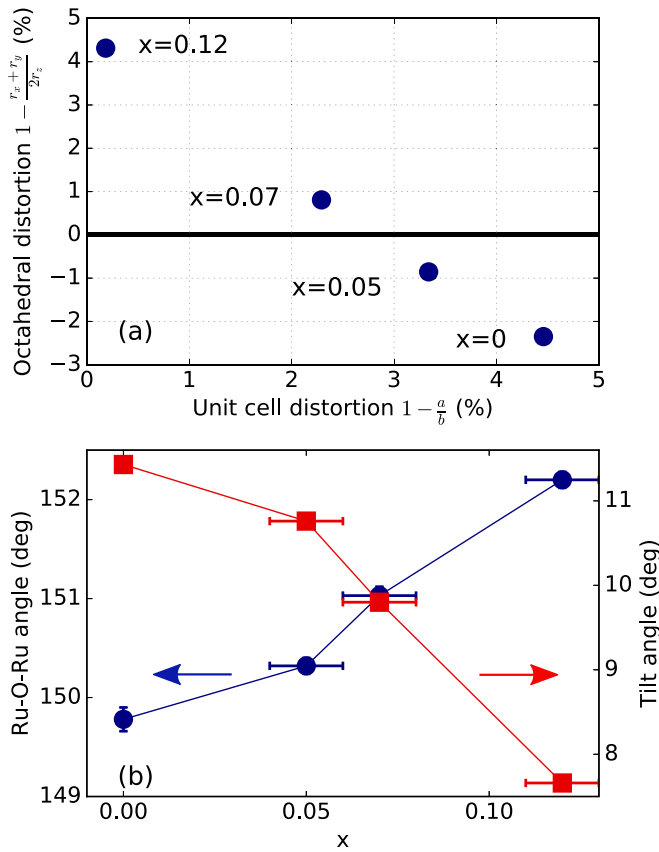


FIG. 3. Structural changes of $\text{Ca}_{2-x}\text{La}_x\text{RuO}_4$ as a function of doping at $T = 10$ K. (a) Phase diagram as a function of the RuO_6 octahedra distortion $1 - \frac{r_x+r_y}{2r_z}$ (with $r_{x,y}$ and r_z in-plane and apical Ru-O bond length, respectively) and unit cell distortion $1 - \frac{a}{b}$ (a, b in-plane lattice parameters of the Pbca unit cell). The horizontal line separates the regions corresponding to octahedral compression ($1 - \frac{r_x+r_y}{2r_z} < 0$) and elongation ($1 - \frac{r_x+r_y}{2r_z} > 0$). (b) Ru-O-Ru bond angle (circles) and RuO_6 octahedra tilt angle away from the \mathbf{c} axis (squares) as a function of the La content. The horizontal error bars reflect the uncertainty in the doping level measured by means of EDX.

B. Magnetic structure

The globally AFM A-centred and weakly FM B-centred modes [see Fig. 1(b)] give rise to two separate sets of AFM space-group forbidden reflections (Table I) for moments along the \mathbf{b} axis [19,40], which can be selectively accessed in a scattering experiment. The AFM coupling of the net magnetization induced by the moment canting between consecutive RuO_2 layers in the A-centred structure [Fig. 1(b)] results in additional weak magnetic reflections (not listed in Table I): the signal at the corresponding (hkl) values, however, was found

TABLE I. Space-group forbidden magnetic reflections arising from the main AFM order of the two magnetic modes in Ca_2RuO_4 [19,40].

	AFM reflections
A-centred mode	(100), (011), (013), (120)
B-centred mode	(010), (101), (012), (103), (014)

[30] to be dominated by anisotropic tensor of susceptibility (ATS) scattering [41]. In contrast to the previous REXS study on the parent compound [42], where the (100) magnetic reflection was probed, our scattering geometry limited our investigation to the magnetic diffraction peaks with a nonzero l component [i.e., of the type $(h0l)$ or $(0kl)$].

The energy dependence of the (013) magnetic peak (A-centred mode) in the parent compound is reported in Fig. 4(a). The data have been corrected for self-absorption using the corresponding XANES signal [30] [also shown in Fig. 4(a)]. As already reported by Zegkinoglou *et al.* [42], a strong resonant enhancement of the diffracted intensity is present at both the Ru L_3 and L_2 absorption edges. This contrasts with the case of iridium oxides with the perovskite structure, where the Ir L_2 resonance is absent due to the strong SOC of $5d$ electrons [43–45]. The Ru resonance originates from electric dipole $2p \rightarrow 4d$ transitions which directly probe the partially filled Ru $4d$ states responsible for magnetism. Each resonance displays two distinct features residing at $E = 2.8383(2), 2.8417(2)$ keV (L_3) and $E = 2.9674(2), 2.9721(2)$ keV (L_2), which arise from transitions to the crystal-field-split t_{2g} and e_g Ru $4d$ orbitals, respectively [42]. The (013) signal is largely magnetic in origin as demonstrated by its temperature (Fig. 5), polarization [Fig. 6(a)] and azimuthal dependence [Fig. 7(a)]. A small contribution from ATS scattering might also be present [30], as evidenced by the weak diffracted signal observed above the Néel temperature (see blue circles in Fig. 5) and the residual intensity in the $\sigma - \sigma'$ polarization channel [Fig. 6(a)]. The latter is also partially accounted for by the leakage from the $\sigma - \pi'$ channel, caused by the fact that the scattering angle of the analyzer crystal was not exactly 90° .

As well as the (013), a large energy resonance was also found for the (011) A-centred reflection [30]. Several B-centred peaks (Table I) were also investigated at various sample azimuth values, but no significant diffracted intensity was detected in the parent compound. This is clearly shown in Fig. 8(a), where the (013) and (014) self-absorption corrected Ru L_3 resonances at low temperature are reported on the same scale. The (014) intensity is negligible and mostly resonates at the e_g levels energy, thus suggesting that the signal is dominated by weak ATS scattering. This is consistent with previous neutron scattering measurements [19], which found a prevalence of the A-centred mode.

In order to verify whether the magnetic structure of the parent compound is retained upon La substitution, we probed several A-centred and B-centred magnetic reflections in the doped samples. A significant diffracted intensity was found at the same $\mathbf{k} = (0,0,0)$ reflections. However, in stark contrast to the undoped crystal, a large resonance is present for the B-centred peaks only [Fig. 8(b)]. The B-centred resonances display similar features to the A-centred ones in the parent compound, as illustrated in Figs. 4(b) and 4(c) for the (014) reflection. In particular, a double $t_{2g} - e_g$ peak with a comparable resonant enhancement is present at both the Ru L_3 and L_2 edge. A minor exception is represented by the weaker L_2 (014) resonance in the $x = 0.07$ sample, which could be attributed to changes in the Ru^{4+} electronic levels induced by doping (see Sec. V). It should be noticed, however, that the resonant enhancement of the (103) magnetic reflection at the two edges is similar to the one observed at lower La content

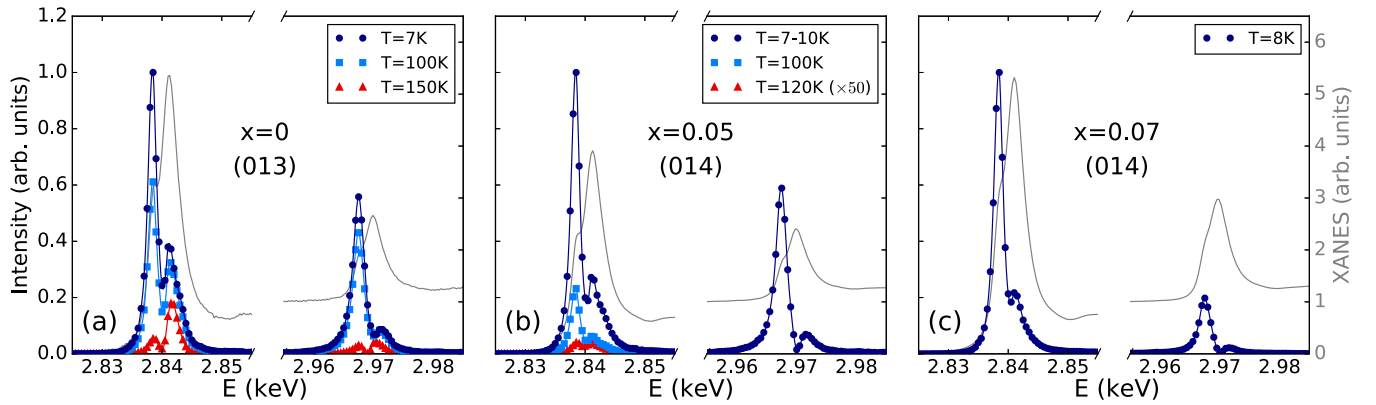


FIG. 4. Ru L_3 and L_2 energy resonances of magnetic diffraction peaks at different temperatures across the Néel transition in the (a) undoped, (b) $x = 0.05$ and (c) 0.07 sample. The filled symbols refer to the total scattered intensity corrected for self-absorption and normalized to the L_3 peak intensity for each sample. The solid lines represent a quadratic interpolation to the data points and are meant just as a guide to the eye. The data were measured at $\psi = 0^\circ$ for $x = 0$ and 0.05 at $T = 100, 120$ K, while the low-temperature $x = 0.05$ and 0.07 data sets correspond to an average of the spectra collected in the range $\psi = 0^\circ - 60^\circ$ and at $\psi = 0^\circ$ and 30° , respectively [30]. The normalized XANES used for the self-absorption correction is also shown.

[30]: therefore a definitive conclusion on the impact of doping on the Ru^{4+} electronic structure cannot be drawn from the data of Fig. 4.

The B-centred mode was found to be predominant across the whole crystal without any significant spatial dependence. This is shown in the color maps of Fig. 9, where the spatial dependence of the magnetic (014) diffraction peak in the $x = 0.05$ crystal is reported along with the one of the (004) Bragg peak. The measurements were performed translating the sample under the beam focal spot and collecting a rocking scan in each position. The size of the incident beam was reduced to $0.1 \times 0.1 \text{ mm}^2$ through a set of slits. The (014) intensity shows limited variations throughout the measured sample area, with minor changes resulting from trivial inhomogeneities in the crystal quality across the sample [as can be seen from the comparison to the (004) map]. This excludes the presence of phase-separated domains of prevalent A or B character.

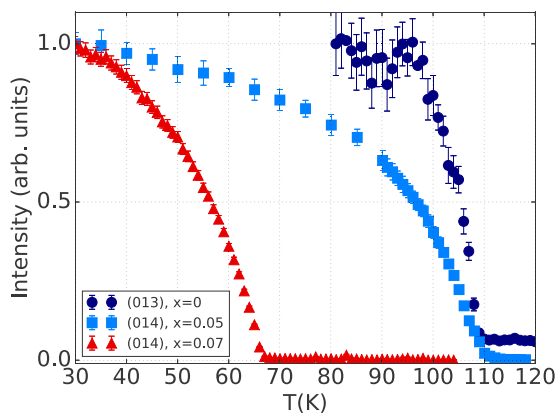


FIG. 5. Temperature dependence of the (013) (dark blue circles) and (014) magnetic diffraction peaks in the undoped and $x = 0.05$ (light blue squares) and $x = 0.07$ (red triangles) samples, respectively. The data points correspond to the total diffracted intensity integrated over a rocking curve at $E = 2.838 \text{ keV}$ and $\psi = 0^\circ$ and normalized to the low-temperature value.

In addition to the resonant enhancement, the magnetic origin of the $\mathbf{k} = (0,0,0)$ space-group forbidden reflections in the doped samples is strongly supported by the fact that (i) the scattered intensity vanishes upon warming beyond $T_N \approx 110 \text{ K}$ ($T_N \approx 70 \text{ K}$) in the $x = 0.05$ ($x = 0.07$) sample and (ii) the scattered signal is predominantly π' polarized [Figs. 6(b) and 6(c)] regardless of the x-ray energy and ψ value chosen for the measurements [30], as expected for dipole resonant magnetic scattering [32]. As for the parent compound, the weak intensity in the $\sigma - \sigma'$ polarization channel is due to leakage from the $\sigma - \pi'$ channel and σ' -polarized ATS scattering. The azimuthal dependence of the (014) [Fig. 7(b)] and (103) (see Ref. [30]) reflections is also consistent with the calculations performed assuming the C-AFM structure with \mathbf{b} -axis moments reported for pure Ca_2RuO_4 [19].

V. DISCUSSION

Our results clearly show that the doped samples retain the same $\mathbf{k} = (0,0,0)$ C-AFM structure of the parent compound. In particular, as shown by the azimuthal dependence of Fig. 7, the Ru^{4+} moments preserve their \mathbf{b} alignment. The impact of La substitution is limited to a suppression of the globally AFM A-centred mode, predominant in the parent compound, and a concomitant stabilisation of the B-centred structure, where a weak net magnetization is present as a result of the FM alignment of the canting-induced net moments. A similar effect has been reported both in $\text{Ca}_{2-x}\text{Sr}_x\text{RuO}_4$ [26] and Ca_2RuO_4 under pressure [46]. Contrary to the La case, Sr and Ca are both divalent: Sr doping thus only realizes a bandwidth control of the parent insulator, due to the different Shannon radii of the Sr^{2+} ($r = 1.31 \text{ \AA}$) and Ca^{2+} ($r = 1.18 \text{ \AA}$) ions [38]. Moreover, the internal chemical pressure originating from Sr doping and the application of external pressure have similar structural effects [46]. The latter also resemble our neutron scattering results and therefore suggest that the changes in the crystal structure may be responsible for the observed transition from A- to B-type order. In this respect, the evolution of the Ru-O-Ru bond angle upon doping could be of particular importance since it

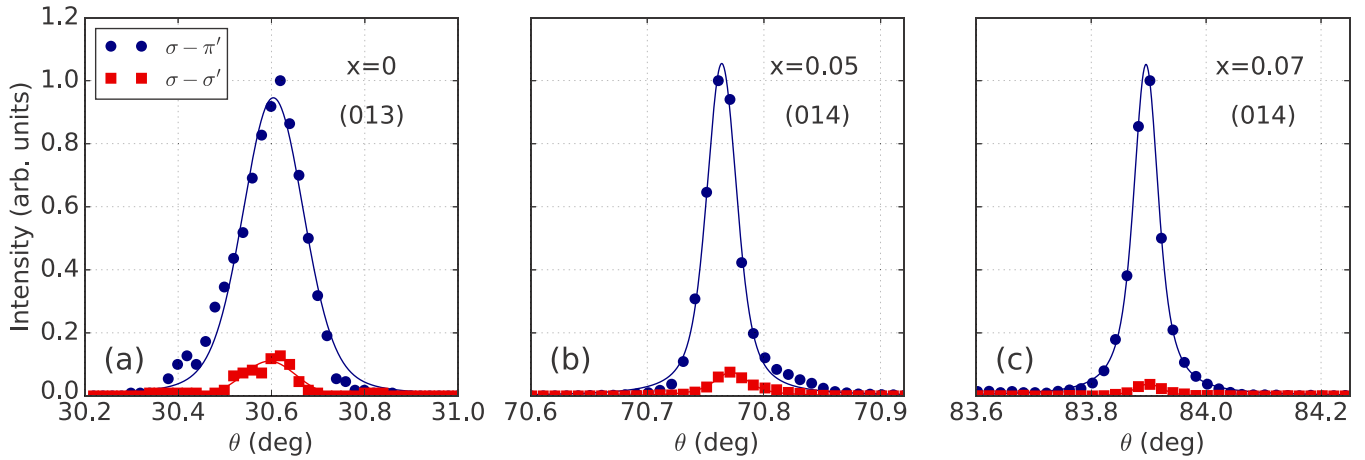


FIG. 6. Polarization dependence of magnetic diffraction peaks in the (a) undoped, (b) $x = 0.05$ and (c) 0.07 sample at $T = 7 - 8$ K. The filled symbols refer to the scattered intensity measured over a rocking scan in the $\sigma - \pi'$ (blue circles) and $\sigma - \sigma'$ (red squares) channels of the polarization analyser crystal normalized to the $\sigma - \pi'$ peak intensity, while the solid lines represent a fit to Voigt profile. The data were collected at $E = 2.838$ keV and $\psi = 110^\circ, 50^\circ, 30^\circ$ for $x = 0, 0.05, 0.07$, respectively.

directly controls the oxygen-mediated superexchange between Ru atoms[47]. This could favor the FM alignment of the net moments and might be one of the mechanisms involved in the stabilisation of the B-centred structure.

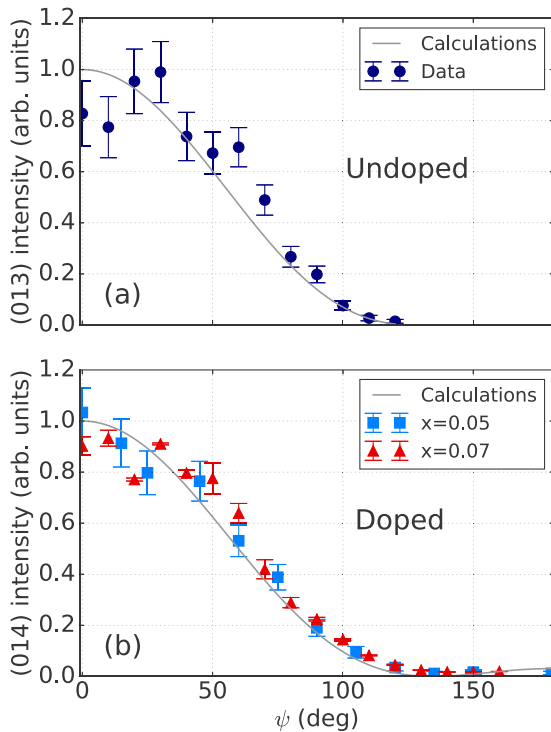


FIG. 7. Azimuthal dependence [azimuthal reference (010)] of the (013) and (014) magnetic diffraction peaks in the (a) undoped and (b) doped ($x = 0.05, 0.07$) samples at $T = 7 - 8$ K, respectively. The filled symbols refer to the scattered intensity integrated over a rocking curve at $E = 2.838$ keV corrected for the geometry-dependent self-absorption factor [30]. The solid lines represent the calculated azimuthal dependence (except for an arbitrary scale factor) assuming the C-AFM structure with \mathbf{b} -axis moments reported by Braden *et al.* [19]. The intensity is normalized to the calculated value at $\psi = 0^\circ$.

The ground-state wave function of the Ru^{4+} ion was described in terms of an admixture of xy , yz , and zx orbitals, whose respective contribution depends on the relative strength of the tetragonal crystal field δ and SOC λ [20,48–53]. Within this picture, the tuning of the crystal field caused by the elongation of the RuO_6 octahedra [Fig. 3(a)] is expected to result in an enhanced xy hole occupancy in the doped compounds with respect to the parent case. This is indeed what was reported for $\text{Ca}_{2-x}\text{Sr}_x\text{RuO}_4$: here, the orbital degeneracy control achieved by Sr doping shifts the Ru $4d$ xy bands towards the Fermi level and turns the AFM exchange of the parent compound into a FM one at $x_c = 0.5$ [49,54]. A similar effect might be present also in the case of La doping and contribute to the stabilisation of the B-centred structure. Moreover, Hartree-Fock calculations [20,52] predicted that the increase in the xy holes population driven by tetragonal elongation should result into a z alignment of the Ru magnetic moments. Although the presence of a finite z component cannot be excluded by our measurements, a spin-flop transition to a c -axis AFM structure in the tetragonally elongated $x = 0.07$ sample is ruled out by the azimuthal dependence of the scattered intensity [Fig. 7(b)].

The evolution from A- to B-type magnetic order naturally explains the FM behavior seen in bulk magnetization measurements [27–29] as resulting from the weak FM component of the B-centred C-AFM mode, rather than a doping-induced local FM alignment (FM polarons) of Ru moments[28,29]. This is consistent with the interpretation given by Fukazawa *et al.* [27] based on their SQUID data. Given their sensitivity to the macroscopic magnetization of the sample, bulk measurements alone are not capable of unequivocally distinguishing between the two scenarios: similar results are indeed expected regardless of whether the magnetization arises from a FM ordering with a small ordered moment or an AFM structure with a weak net magnetization due to moments canting. A further confirmation comes from the measurements performed on nonstoichiometric $\text{Ca}_2\text{RuO}_{4+\delta}$ [19]: here, a B-type C-AFM structure was also found and the bulk magnetization shows similar features to the ones of the La-doped compounds. The increase in the net moment seen for increasing levels of La

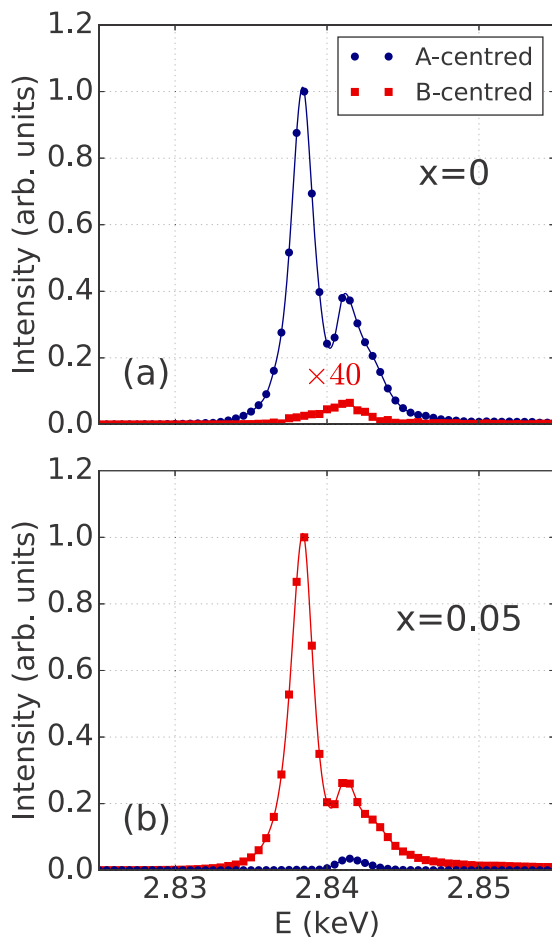


FIG. 8. Comparison between the (013) (blue circles) and (014) (red squares) Ru L_3 resonances in the (a) undoped and (b) $x = 0.05$ sample. The filled symbols refer to the total scattered intensity at $T = 7-8$ K corrected for self-absorption and normalized to the peak intensity of the dominant mode. The solid lines represent a quadratic interpolation to the data points and are meant just as a guide to the eye. The data were measured at $\psi = 0^\circ$, apart from the (014) in the undoped sample, for which $\psi = 80^\circ$.

content [28] is also compatible with the C-AFM scenario, where it could arise from an increase of either the B-centred mode volume fraction or the DMI-induced canting angle. However, minor changes in the magnitude of the latter could not be investigated since the resulting weak FM component, contrary to the case of the A-centred mode, does not give rise to any space-group forbidden reflections.

Although most of the literature on $\text{Ca}_{2-x}\text{La}_x\text{RuO}_4$ focuses on the filling control of the Ru $4d$ bands associated with the extra electron introduced by the La^{3+} ion [14,27–29], our findings show that the concomitant structural effects are likely to play a crucial role in the physics of the system. This scenario is somewhat confirmed by recent resistivity and ARPES measurements on Pr-doped Ca_2RuO_4 [39], which suggest that, in contrast to lightly doped cuprates [55] and iridates [56,57], the doped electrons remain fully localized in the $S\text{-}Pbca$ phase irrespective of the Pr content. A pronounced sensitivity to the doping-induced structural changes is also expected in light of the importance of lattice energies in the stabilization of the

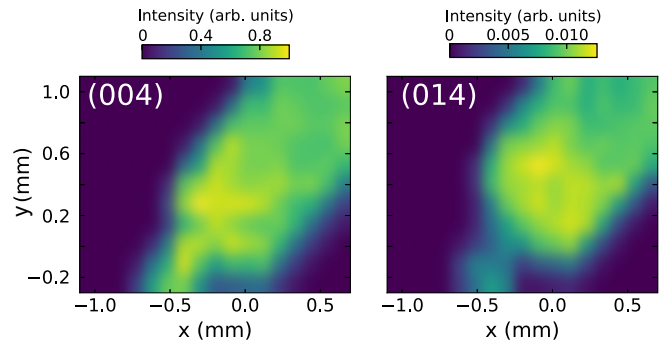


FIG. 9. Intensity maps of the (004) Bragg peak and (014) magnetic reflection ($T = 8$ K, $\psi = 0^\circ$) in the $x = 0.05$ sample as a function of the incident x-ray beam position on the crystal (beam size 0.1×0.1 mm 2). The color scale represents the integrated intensity over a rocking scan measured in each position normalized to the (004) peak value (the dark regions are off the sample).

low-temperature insulating state highlighted by recent *ab initio* calculations in the parent compound [58].

Nonetheless, $\text{Ca}_{2-x}\text{La}_x\text{RuO}_4$ was explicitly reported as an example of an electron-doped system in recent theoretical calculations [14]. The latter found that the impact of the injection of free carriers on the ground state of d^4 Mott insulators dramatically depends on the interplay between the exchange interaction K , the hopping integral t_0 and the SOC constant λ . In particular, starting from the parent compound AFM ground state, a FM phase is predicted to rapidly appear upon electron doping for sufficiently weak SOC. This scenario has been explicitly supported by Chaloupka and Khaliullin [14] who, backed by the interpretation of the bulk magnetization data given by Cao *et al.* [28], based their conclusion on previous estimates for λ [11,20]. Our measurements, however, show that the FM phase is not realized in $\text{Ca}_{2-x}\text{La}_x\text{RuO}_4$. AFM order survives up to $x = 0.07(1)$, while the system is found to be PM at $x = 0.12(1)$. Assuming the filling of the Ru $4d$ bands is the dominant effect in the physics of La-doped Ca_2RuO_4 , this sets a lower boundary to the SOC constant: considering $t_0 \approx 300$ meV [14], the FM phase is predicted to be absent for $\lambda > 77$ meV. The latter estimate is compatible with the value $\lambda \approx 200$ meV from a recent O K -edge RIXS investigation[48]. Approximating to $x = 0.10$ the value of the doping level at which the transition between the C-AFM and PM states occurs [27], the phase diagram of Ref. [14] gives $\lambda \approx 400$ meV. This is comparable to the value found for $5d$ transition metal oxides [59] and thus seems overestimated. The theoretical phase diagram of Ref. [14], however, neglects the structural changes discussed in the present investigation (as well as distortions away from the perfect cubic symmetry of the RuO_6 octahedra and deviations from two-dimensionality) and, as a result, it does not provide with an accurate description of the physics of $\text{Ca}_{2-x}\text{La}_x\text{RuO}_4$.

VI. CONCLUDING REMARKS

In conclusion, our REXS investigation establishes the persistence of the C-AFM structure of the parent compound in $\text{Ca}_{2-x}\text{La}_x\text{RuO}_4$. The AFM order was found to be present up

to $x = 0.07(1)$, while long-range order is absent in the $x = 0.12(1)$ sample. La substitution suppresses the globally AFM A-centred mode, dominant in pure Ca_2RuO_4 , and favours the B-centred structure, which displays a weak net magnetization as a result of the moments canting. The latter naturally explains the net magnetization observed in previously published bulk magnetization measurements on the doped samples. Our results rule out the presence of a FM phase and also suggest that the structural changes, which accompany La doping are likely to play a pivotal role in the observed magnetic properties and should be considered alongside the electron doping effect in any meaningful description of the physics of the system.

ACKNOWLEDGMENTS

The authors would like to thank the I10 beamline staff at DLS for their help during the bulk magnetization measurements. We acknowledge Diamond Light Source for time on beamline I16 under Proposals No. MT-15323, No. MT-15952, No. MT-15867, and No. MT-18934. Experiments at the ISIS Neutron and Muon Source were supported by a beamtime allocation from the Science and Technology Facilities Council. This work is supported by the UK Engineering and Physical Sciences Research Council (Grants No. EP/N027671/1, No. EP/N034694/1 and No. EP/N034872/1) and by the Swiss National Science Foundation (Grant No. 200021_153405).

-
- [1] P. A. Lee, N. Nagaosa, and X. G. Wen, *Rev. Mod. Phys.* **78**, 17 (2006).
- [2] M. Imada, A. Fujimori, and Y. Tokura, *Rev. Mod. Phys.* **70**, 1039 (1998).
- [3] X. Chen, T. Hogan, D. Walkup, W. Zhou, M. Pokharel, M. Yao, W. Tian, T. Z. Ward, Y. Zhao, D. Parshall, C. Opeil, J. W. Lynn, V. Madhavan, and S. D. Wilson, *Phys. Rev. B* **92**, 075125 (2015).
- [4] H. Gretarsson, N. H. Sung, J. Porras, J. Bertinshaw, C. Dietl, J. A. N. Bruin, A. F. Bangura, Y. K. Kim, R. Dinnebier, J. Kim, A. Al-Zein, M. Moretti Sala, M. Krisch, M. Le Tacon, B. Keimer, and B. J. Kim, *Phys. Rev. Lett.* **117**, 107001 (2016).
- [5] X. Liu, M. P. M. Dean, Z. Y. Meng, M. H. Upton, T. Qi, T. Gog, Y. Cao, J. Q. Lin, D. Meyers, H. Ding, G. Cao, and J. P. Hill, *Phys. Rev. B* **93**, 241102(R) (2016).
- [6] D. Pincini, J. G. Vale, C. Donnerer, A. de la Torre, E. C. Hunter, R. Perry, M. Moretti Sala, F. Baumberger, and D. F. McMorrow, *Phys. Rev. B* **96**, 075162 (2017).
- [7] S. W. Cheong, G. Aeppli, T. E. Mason, H. Mook, S. M. Hayden, P. C. Canfield, Z. Fisk, K. N. Clausen, and J. L. Martinez, *Phys. Rev. Lett.* **67**, 1791 (1991).
- [8] B. Vignolle, S. M. Hayden, D. F. McMorrow, H. M. Rønnow, B. Lake, C. D. Frost, and T. G. Perring, *Nat. Phys.* **3**, 163 (2007).
- [9] M. Fujita, H. Hiraka, M. Matsuda, M. Matsuura, J. M. Tranquada, S. Wakimoto, G. Xu, and K. Yamada, *J. Phys. Soc. Jpn.* **81**, 011007 (2012).
- [10] X. Chen, J. L. Schmeh, Z. Islam, Z. Porter, E. Zoghlin, K. Finkelstein, J. P. C. Ruff, and S. D. Wilson, *Nat. Commun.* **9**, 103 (2018).
- [11] A. Abragam and B. Bleaney, *Electron Paramagnetic Resonance of Transition Ions* (Clarendon, Oxford, 1970).
- [12] D. I. Khomskii, *Transition Metal Compounds* (Cambridge University Press, Cambridge, 2014), p. 485.
- [13] G. Khaliullin, *Phys. Rev. Lett.* **111**, 197201 (2013).
- [14] J. Chaloupka and G. Khaliullin, *Phys. Rev. Lett.* **116**, 017203 (2016).
- [15] A. Jain, M. Krautloher, J. Porras, G. H. Ryu, D. P. Chen, D. L. Abernathy, J. T. Park, A. Ivanov, J. Chaloupka, G. Khaliullin, B. Keimer, and B. J. Kim, *Nat. Phys.* **13**, 633 (2017).
- [16] S. Kunkemöller, D. Khomskii, P. Steffens, A. Piovano, A. A. Nugroho, and M. Braden, *Phys. Rev. Lett.* **115**, 247201 (2015).
- [17] S. Kunkemöller, E. Komleva, S. V. Streltsov, S. Hoffmann, D. I. Khomskii, P. Steffens, Y. Sidis, K. Schmalzl, and M. Braden, *Phys. Rev. B* **95**, 214408 (2017).
- [18] G. Zhang and E. Pavarini, *Phys. Rev. B* **95**, 075145 (2017).
- [19] M. Braden, G. André, S. Nakatsuji, and Y. Maeno, *Phys. Rev. B* **58**, 847 (1998).
- [20] T. Mizokawa, L. H. Tjeng, G. A. Sawatzky, G. Ghiringhelli, O. Tjernberg, N. B. Brookes, H. Fukazawa, S. Nakatsuji, and Y. Maeno, *Phys. Rev. Lett.* **87**, 077202 (2001).
- [21] S. Nakatsuji and Y. Maeno, *J. Low Temp. Phys.* **117**, 1593 (1999).
- [22] H. J. Noh, S. J. Oh, B. G. Park, J. H. Park, J. Y. Kim, H. D. Kim, T. Mizokawa, L. H. Tjeng, H. J. Lin, C. T. Chen, S. Schuppler, S. Nakatsuji, H. Fukazawa, and Y. Maeno, *Phys. Rev. B* **72**, 052411 (2005).
- [23] S. Wang and H. Ding, *New J. Phys.* **7**, 112 (2005).
- [24] J. Baier, P. Steffens, O. Schumann, M. Kriener, S. Stark, H. Hartmann, O. Friedt, A. Revcolevschi, P. G. Radaelli, S. Nakatsuji, Y. Maeno, J. A. Mydosh, T. Lorenz, and M. Braden, *J. Low Temp. Phys.* **147**, 405 (2007).
- [25] P. Steffens, O. Friedt, Y. Sidis, P. Link, J. Kulda, K. Schmalzl, S. Nakatsuji, and M. Braden, *Phys. Rev. B* **83**, 054429 (2011).
- [26] O. Friedt, M. Braden, G. André, P. Adelman, S. Nakatsuji, and Y. Maeno, *Phys. Rev. B* **63**, 174432 (2001).
- [27] H. Fukazawa and Y. Maeno, *J. Phys. Soc. Jpn.* **70**, 460 (2001).
- [28] G. Cao, S. McCall, V. Dobrosavljevic, C. S. Alexander, J. E. Crow, and R. P. Guertin, *Phys. Rev. B* **61**, R5053 (2000).
- [29] G. Cao, C. S. Alexander, S. McCall, J. E. Crow, and R. P. Guertin, *J. Mag. Mag. Mater.*, Proc. Int. Conf. Mag. (ICM 2000), **226–230**, 235 (2001).
- [30] See Supplemental Material at <http://link.aps.org/supplemental/10.1103/PhysRevB.98.014429> for additional data and further details on the data analysis.
- [31] S. P. Collins, A. Bombardi, A. R. Marshall, J. H. Williams, G. Barlow, A. G. Day, M. R. Pearson, R. J. Woolliscroft, R. D. Walton, G. Beutier, and G. Nisbet, in *Proceedings of the 10th International Conference on Synchrotron Radiation Instrumentation*, edited by R. Garrett, I. Gentle, K. Nugent, and S. Wilkins, AIP Conf. Proc. No. 1234 (AIP, Melbourne, 2010), pp. 303–306.
- [32] J. P. Hill and D. F. McMorrow, *Acta Crystallogr. Sect. A* **52**, 236 (1996).

- [33] D. A. Keen, M. J. Gutmann, and C. C. Wilson, *J. Appl. Crystallogr.* **39**, 714 (2006).
- [34] S. Nakatsuji, S.-i. I. Ikeda, and Y. Maeno, *J. Phys. Soc. Jpn.* **66**, 1868 (1997).
- [35] C. S. Alexander, G. Cao, V. Dobrosavljevic, S. McCall, J. E. Crow, E. Lochner, and R. P. Guertin, *Phys. Rev. B* **60**, R8422 (1999).
- [36] G. Cao, S. McCall, M. Shepard, J. E. Crow, and R. P. Guertin, *Phys. Rev. B* **56**, R2916 (1997).
- [37] H. Fukazawa, S. Nakatsuji, and Y. Maeno, *Physica B* **281-282**, 613 (2000).
- [38] R. D. Shannon, *Acta Crystallogr. Sect. A* **32**, 751 (1976).
- [39] S. Riccò, M. Kim, A. Tamai, S. M. Walker, F. Y. Bruno, I. Cucchi, E. Cappelli, C. Besnard, T. K. Kim, P. Dudin, M. Hoesch, M. Gutmann, A. Georges, R. S. Perry, and F. Baumberger, [arXiv:1803.00488](https://arxiv.org/abs/1803.00488).
- [40] D. G. Porter, V. Granata, F. Forte, S. Di Matteo, M. Cuoco, R. Fittipaldi, A. Vecchione, and A. Bombardi, [arXiv:1807.00721](https://arxiv.org/abs/1807.00721).
- [41] V. E. Dmitrienko, *Acta Crystallogr. Sect. A* **39**, 29 (1983).
- [42] I. Zegkinoglou, J. Stremper, C. S. Nelson, J. P. Hill, J. Chakhalian, C. Bernhard, J. C. Lang, G. Srajer, H. Fukazawa, S. Nakatsuji, Y. Maeno, and B. Keimer, *Phys. Rev. Lett.* **95**, 136401 (2005).
- [43] B. J. Kim, H. Ohsumi, T. Komesu, S. Sakai, T. Morita, H. Takagi, and T. Arima, *Science* **323**, 1329 (2009).
- [44] S. Boseggia, R. Springell, H. C. Walker, C. Rüegg, H. Okabe, M. Isobe, R. S. Perry, S. P. Collins, and D. F. McMorrow, *Phys. Rev. Lett.* **110**, 117207 (2013).
- [45] M. Moretti Sala, S. Boseggia, D. F. McMorrow, and G. Monaco, *Phys. Rev. Lett.* **112**, 026403 (2014).
- [46] P. Steffens, O. Friedt, P. Alireza, W. G. Marshall, W. Schmidt, F. Nakamura, S. Nakatsuji, Y. Maeno, R. Lengsdorf, M. M. Abd-Elmeguid, and M. Braden, *Phys. Rev. B* **72**, 094104 (2005).
- [47] J. B. Goodenough, in *Magnetism and the Chemical Bond*, edited by F. A. Cotton, G. A. Olah, and I. Prigogine, Interscience Monographs Chemistry (John Wiley & Sons, New York, London, 1963).
- [48] C. G. Fatuzzo, M. Dantz, S. Fatale, P. Olalde-Velasco, N. E. Shaik, B. Dalla Piazza, S. Toth, J. Pellicciari, R. Fittipaldi, A. Vecchione, N. Kikugawa, J. S. Brooks, H. M. Rønnow, M. Grioni, C. Rüegg, T. Schmitt, and J. Chang, *Phys. Rev. B* **91**, 155104 (2015).
- [49] S. Nakatsuji and Y. Maeno, *Phys. Rev. B* **62**, 6458 (2000).
- [50] G. Q. Liu, *Phys. Rev. B* **84**, 235136 (2011).
- [51] G. Q. Liu, *Phys. Rev. B* **88**, 104428 (2013).
- [52] M. Kurokawa and T. Mizokawa, *Phys. Rev. B* **66**, 024434 (2002).
- [53] L. Das, F. Forte, R. Fittipaldi, C. G. Fatuzzo, V. Granata, O. Ivashko, M. Horio, F. Schindler, M. Dantz, Y. Tseng, D. E. McNally, H. M. Rønnow, W. Wan, N. B. Christensen, J. Pellicciari, P. Olalde-Velasco, N. Kikugawa, T. Neupert, A. Vecchione, T. Schmitt, M. Cuoco, and J. Chang, *Phys. Rev. X* **8**, 011048 (2018).
- [54] Z. Fang, N. Nagaosa, and K. Terakura, *Phys. Rev. B* **69**, 045116 (2004).
- [55] A. Damascelli, Z. Hussain, and Z.-X. Shen, *Rev. Mod. Phys.* **75**, 473 (2003).
- [56] A. de la Torre, S. McKeown Walker, F. Y. Bruno, S. Riccò, Z. Wang, I. Gutierrez Lezama, G. Scheerer, G. Giriat, D. Jaccard, C. Berthod, T. K. Kim, M. Hoesch, E. C. Hunter, R. S. Perry, A. Tamai, and F. Baumberger, *Phys. Rev. Lett.* **115**, 176402 (2015).
- [57] Y. K. Kim, O. Krupin, J. D. Denlinger, A. Bostwick, E. Rotenberg, Q. Zhao, J. F. Mitchell, J. W. Allen, and B. J. Kim, *Science* **345**, 187 (2014).
- [58] Q. Han and A. Millis, [arXiv:1801.06215](https://arxiv.org/abs/1801.06215).
- [59] B. J. Kim, H. Jin, S. J. Moon, J.-Y. Kim, B.-G. Park, C. S. Leem, J. Yu, T. W. Noh, C. Kim, S.-J. Oh, J. H. Park, V. Durairaj, G. Cao, and E. Rotenberg, *Phys. Rev. Lett.* **101**, 076402 (2008).